Aeroelastic Stability of Periodic Systems with Application to Rotor Blade Flutter

P. FRIEDMANN* AND L. J. SILVERTHORN†
University of California, Los Angeles, Calif.

The dynamics of a helicopter blade in forward flight are described by a system of linear differential equations with periodic coefficients. The stability of this periodic aeroelastic system is determined using multivariable Floquet-Liapunov theory. The transition matrix at the end of the period is evaluated by a) direct numerical integration, and b) a new, approximate method, which consists of approximating a periodic function by a series of step functions. The numerical accuracy and efficiency of the methods is compared and the second method is shown to be superior by far. Results illustrating the effect of the periodic coefficients and various blade parameters are presented.

Nomenclature

a = two-dimensional lift curve slope
$\mathbf{A}(\psi)$ = periodic matrix, defined in Appendix A
A_{F1}, A_{L1} = generalized aerodynamic load for first flap and lag mode, respectively
$\bar{B}^i$ = generalized mass, described in Appendix A
$\mathbf{C}_k$ = constant matrix approximation of $\mathbf{A}(\psi)$ over kth interval
$\mathbf{C}(\psi, K)$ = step function approximation to $\mathbf{A}(\psi)$
C_{do} = profile drag coefficient
$C(k)$ = Theodorsen's lift deficiency function
e_1 = blade pitch bearing offset defined in Fig. 1
$\bar{E}_{11}{}^s, \bar{E}_{11}{}^s$ = terms associated with the elastic coupling effect described in Appendix A
$\bar{E}_{11}{}^{cs}, \bar{E}_{11}{}^{cs}$
F^i = flap coefficients (Appendix A)
g_1 = generalized coordinate, first normal flap mode
$g_1{}^o$ = static value of g_1 in hover
Δg_1 = perturbation in g_1 about $g_1{}^o$
$\mathbf{H}(K)$ = approximate transition matrix at end of period
h_1 = generalized coordinate, first normal inplane mode
$h_1{}^o$ = static value of h_1 in hover
Δh_1 = perturbation in h_1 about $h_1{}^o$
$\mathbf{i}, \mathbf{j}, \mathbf{k}$ = unit vectors in x, y, and z directions (Fig. 1)
$\mathbf{I}$ = unit matrix
l = length of blade capable of elastic deflection
L^i = lag coefficients (Appendix A)
$\bar{M}_{F1}, \bar{M}_{L1}$ = generalized mass for first flap and lag mode, respectively
$(\bar{M}_\eta)_{111}, (\bar{M}_\gamma)_{111}$ = described in Appendix A
$\bar{P}_{111}$ = described in Appendix A
R = blade radius
$\mathbf{Q}$ = constant matrix
T = common nondimensional period
u, v, w = x, y, and z displacement of a point on the elastic axis of the blade
$U(\psi)$ = heaviside unit step function
v_e, v_{eo} = elastic part of the displacement of a point on the elastic axis (Fig. 1), v_{eo} static value of v_e
w_e, w_{eo} = elastic part of the displacement of a point on the elastic axis (Fig. 1), w_{eo} static value of w_e
$x_o = x - e_1$
x, y, z = rotating orthogonal coordinate system
$\mathbf{y}(\psi)$ = state variable column matrix
$\mathbf{y}_A(\psi, K)$ = approximate value of $\mathbf{y}(\psi)$
$(\bar{\ })$ = nondimensionalized quantity
$(\ )_R, (\ )_I$ = subscripts denote real and imaginary part of appropriate quantity
$(\boldsymbol{\rho})^{-1}$ = boldface quantities with a $^{-1}$ denote inverse of a matrix
$(*)$ = differentiation with respect to ψ
α = angle of reversed flow region (Fig. 2)
β_D = droop, built in angle of the undeformed position of the blade measured from the feathering axis (Fig. 1)
β_P = preconing, inclination of the feathering axis with respect to the hub plane (Fig. 1)
γ = lock number $\gamma = (2\rho_A bR^5 a/I_b)$ based on normal flow
γ_1 = first inplane bending mode
ϵ_D = symbolic quantity having the same order of magnitude as the displacements v and w
ζ_k = real part of the kth characteristic exponent
η_1 = first flapwise bending mode
η_{SF1}, η_{SL1} = viscous structural damping coefficients, in percent of critical damping, for first flap and lag mode, respectively
θ = collective pitch angle measured from x-y plane
λ = inflow ratio, induced velocity over disk, positive down, nondimensionalized with respect to $R\Omega$
$\boldsymbol{\lambda}$ = diagonal matrix, containing eigenvalues λ_k of $\mathbf{R}$
$\boldsymbol{\Lambda}$ = diagonal matrix containing eigenvalues Λ_k of $\Phi(T, 0)$
= advanced ratio
μ_c = critical value of u, at which the system becomes unstable
ρ_A = density of air
ξ_k = dummy variable in kth interval
σ = blade solidity ratio
$\boldsymbol{\Phi}(\psi, \psi_o)$ = fundamental matrix at ψ, for initial conditions given at ψ_o, $\Phi_A(\psi, K)$ approximate value of $\Phi(\psi, \psi_o)$
$\boldsymbol{\phi}_k(\psi, \psi_o)$ = kth column of $\Phi(\psi, \psi_o)$, for initial conditions at ψ_o
ψ = azimuth angle of the blade ($\psi = \Omega t$) measured from the straight aft position
ψ_k = value of ψ at end of kth interval
ω_k = imaginary part of kth characteristic exponent
$\bar{\omega}_{F1}, \bar{\omega}_{L1}$ = natural frequency of first flap or lag mode, rotating

Received February 20, 1974; presented as Paper 74-417 at the AIAA/ASME 15th Structures, Structural Dynamics and Materials Conference, Las Vegas, Nev., April 17-19, 1974; revision received May 20, 1974. This work was supported by Langley Directorate, U.S. Army Air Mobility Research and Development Laboratory, Langley Research Center, Hampton, Va., under NASA NGR 05-007-414.

Index categories: Aeroelasticity and Hydroelasticity; VTOL Vibration; Structural Dynamic Analysis.

* Assistant Professor, Mechanics and Structures Department, School of Engineering and Applied Science. Associate Fellow AIAA.

† Research Assistant, Mechanics and Structures Department, School of Engineering and Applied Science; presently Dynamics Engineer, Hughes Helicopter Company, Culver City, Calif.

Introduction

VARIOUS aeroelastic problems are usually modeled mathematically by a system of linear differential equations with periodic coefficients. Some representative problems of this

type are the aeroelastic behavior of a helicopter blade in forward flight, prop-rotor stability in the oblique flight region[1] and the flutter of a panel, in supersonic flow, attached to an oscillating wing.[2]

The purpose of the present study is to apply a numerical method recently developed by Hsu for classical parametric excitation problems,[3-5] and implemented only for relatively simple systems, to the more complicated problem of the aeroelastic stability of a hingeless helicopter blade in forward flight. In particular the numerical efficiency and accuracy of the method will be studied and compared to another method which has been used in the past.

The problem of determining the stability of periodic systems has been treated in the literature associated with various fields such as: a) mathematics, b) linear control system theory, c) dynamic stability or parametric excitation, and d) rotor blade structural dynamics.‡ Unfortunately, a considerable communications gap between researchers working in these areas has led to considerable duplication of efforts. It is the author's belief that the method presented in the present study is one of the most efficient ones available at the present.

Studies dealing with the effect of forward flight (or periodic coefficients) on the aeroelastic behavior of helicopter blades have been primarily devoted to the study of flapping instability at high advance ratios.[1,6-11] A limited number of studies dealing with the effect of periodic coefficients on coupled flap-lag,[12,13] coupled flap-lag-pitch[14] motion were also conducted. The case of coupled flap-lag motion has been, somewhat inconclusively, investigated by Hall[13] using multivariable Floquet theory, the same problem was also considered by Friedmann and Tong[12] but the treatment was limited to low advance ratios ($\mu < 0.3$). The coupled, linearized, flap-lag-torsion motion has been investigated by Crimi[14] using a modified Hill method. In these cases only a limited number of numerical results were presented.

The mathematical methods used in previous studies dealing with the effects of periodic coefficients were: a) the rectangular ripple method,[6] b) analog computer simulation,[7,8] c) various forms of Hill's method,[14] d) multivariable Floquet-Liapunov theory,[1,10,13] and e) perturbation method in multiple time scales.[11,12] The mathematical method used in the present study is the Floquet-Liapunov theorem, and the stability of the system is determined from the eigenvalues of the transition matrix at the end of one period. The transition matrix at the end of one period is computed using two methods: a) Hsu's method, and b) direct numerical integration.

The present study, in addition to demonstrating the effectiveness and efficiency of Hsu's method for calculating the transition matrix of large periodic aeroelastic systems, will also clarify certain important physical aspects of the coupled flap-lag behavior of hingeless blades in forward flight. In particular it will be shown how the flapping behavior is modified by the addition of the lead-lag degree of freedom and the instability due to forward flight (i.e., periodic coefficients) is compared with that in hover. Furthermore, the effect of some important parameters such as: lock number, collective pitch, reversed flow, and combination of rotating flap and lag frequencies on the aeroelastic stability of the blade will be considered.

Equations of Motion

The present study is based upon a consistently derived system of equations of motion for the linearized coupled flap-lag motion of a cantilevered rotor blade at arbitrary advance ratio; the derivation of these equations can be found in Ref. 15. The geometry of the problem is shown in Fig. 1.

The derivation itself is algebraically tedious and will not be given in this paper. However, for the sake of completeness, the assumptions used in deriving this system of equations will be outlined. a) The blade is cantilevered at the hub. It can have an angle of droop β_D at the root. In addition, the feathering axis

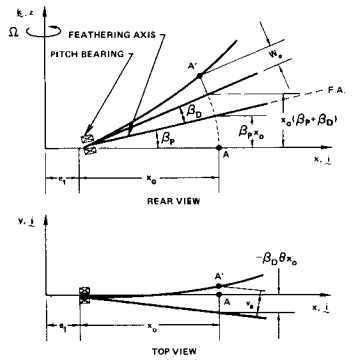

Fig. 1 Displacement field of a torsionally rigid cantilevered rotor blade with droop and preconing.

can be preconed by an angle β_P. The angles β_D and β_P are small. b) The blade can bend in two directions normal to the elastic axis and is torsionally rigid. c) The deflections of the blade are moderately small so that terms of $0(\varepsilon_D{}^2)$ can be neglected compared to one. d) Moderately large deflections have only a small effect on the tension due to elastic effects on the blade since one of its ends is free, thus a linear treatment of the elastic restoring forces is adequate. e) Two-dimensional quasi-steady aerodynamic strip theory is used $C(k) = 1$ and apparent mass effects are neglected. f) Reversed flow is included using an approximate model for reversed flow described in Appendix B (Fig. 2). g) Stall and compressibility effects are neglected. h) A uniform inflow is assumed over the rotor disk. i) Only a collective pitch is applied to the rotor which is not trimmed for forward flight.

Using the assumptions just given a system of nonlinear partial differential equations for the coupled flap-lag motion of the blade is derived, with respect to an x, y, and z coordinate system rotating with the blade (Fig. 1).

Using Galerkin's method for the spatial variable the partial differential equations, derived using the assumptions given above, are reduced to a system of ordinary differential equations. For simplicity these equations are specialized for the case of one elastic mode for each degree of freedom, the equations for an arbitrary number of modes can be found in Ref. 15.

In order to clarify the resulting equations, which will be solved in this paper, the relations for the displacements of the blade are given below

$$u = -w_e(\beta_P+\beta_D) - \frac{x_o}{2}(\beta_P+\beta_D)^2 + V_e\beta_o\theta - \frac{1}{2}\int_o^{x_o}\left[\left(\frac{\partial v_e}{\partial x_1}\right)^2 + \left(\frac{\partial w_e}{\partial x_1}\right)^2\right]dx_1 \tag{1}$$

$$v = v_e - x_o\beta_D\theta$$

$$w = w_e + x_o(\beta_P+\beta_D)$$

$$w_e = l\eta_1 g_1; \quad v_e = -l\gamma_1 h_1$$

With these displacements the equations of coupled flap lag motion of the blade are given by the following ordinary nonlinear equations:

$$\bar{M}_{F1}\overset{**}{g_1} + 2\bar{\omega}_{F1}\bar{M}_{F1}\overset{*}{\eta}_{SF1}g_1 + \bar{E}_{11}{}^{s}g_1 + \bar{\omega}_{F1}{}^{2}\bar{M}_{F1}g_1 = \bar{E}_{11}{}^{cs}h_1 + 2\bar{P}_{111}g_1\overset{*}{h}_1 - (\beta_P+\beta_D)\bar{B}^1 + 2(\beta_P+\beta_D)\bar{B}^3\overset{*}{h}_1 + A_{F1} \tag{2}$$

$$M_{L1}\overset{**}{h_1} + 2M_{L1}\bar{\omega}_{L1}\eta_{SL1}\overset{*}{h}_1 + \bar{M}_{L1}\bar{\omega}_{L1}{}^{2}h_1 - \bar{E}_{11}{}^{s}h_1 = \bar{E}_{11}{}^{cs}g_1 - 2B^7(\beta_P+\beta_D)\overset{*}{g} + \bar{B}^{11}\beta_D\theta + 2[\bar{S}_{111} - (\bar{M})_{111}]\overset{*}{h}_1h_1 - 2(\bar{M}_\eta)_{111}\overset{*}{g}\,g_1 - \bar{B}^{10}\beta_D\theta + A_{L1} \tag{3}$$

where the various quantities used in Eqs. (2-4) are defined in Appendix A.

This system of nonlinear equations is linearized about the steady-state equilibrium position of the blade in hover, the

‡ A brief review of the pertinent literature can be found in Ref. 15.

process of linearization consists of expressing the elastic part of the displacement field as

$$\begin{aligned} w_e &= w_{eo}+\Delta w_e = \eta_1(g_1{}^o+\Delta g_1) \\ v_e &= v_{eo}+\Delta v_e = \eta_1(h_1{}^o+\Delta h_1) \end{aligned} \tag{4}$$

Furthermore, for mathematical convenience, the equations of motion have to be transformed into a system of first-order equations. This is achieved by using the following notation:

$$\left.\begin{aligned} \Delta\overset{*}{g}_1 &= y_1; \quad \Delta\overset{*}{h}_1 = y_3 \\ \Delta g_1 &= y_2; \quad \Delta h_1 = y_4 \end{aligned}\right\} \tag{5}$$

For the stability analysis, only the homogeneous part of the equations of motion is required, thus the equations of motion in their final form can be written as

$$\overset{*}{\mathbf{y}} = \mathbf{A}(\psi)\mathbf{y} \tag{6}$$

where $\mathbf{A}(\psi)$ is a periodic (4×4) matrix defined in Appendix A. Various coefficients in Eq. (6) will have different values in the normal and reversed flow region (see Appendix B).

Method of Solution

Floquet-Liapunov Theorem and Its Consequence

The stability investigation of the blade motions is based upon the Floquet-Liapunov theorem[16] which states the knowledge of the state transition matrix over one period is sufficient in order to determine the stability of a periodic system having a common period T. Based upon the Floquet-Liapunov theorem, the transition matrix for a periodic system, $\mathbf{A}(\psi+T) = A(\psi)$, can be written as

$$\Phi(\psi,\psi_o) = \mathbf{P}^{-1}(\psi)\exp[\mathbf{R}(\psi-\psi_o)]\mathbf{P}(\psi_o) \tag{7}$$

where

$$\mathbf{P}(\psi+T) = \mathbf{P}(\psi) \tag{8}$$

where $\mathbf{R}$ is a constant matrix and $\mathbf{P}(t)$ is a periodic matrix. Clearly the stability of the system is determined by the matrix $\mathbf{R}$, where $\mathbf{R}$ is given by following relation:

$$\Phi(T,0) = \exp(\mathbf{R}T) \tag{9}$$

A direct result of the Floquet-Liapunov theorem is that the knowledge of the transition matrix over one period determines the solution to the homogeneous system everywhere through the relation

$$\Phi(\psi+sT,0) = \Phi(\psi,0)[\exp(\mathbf{R}T)]^s \tag{10}$$

where $0 \leqq \psi \leqq T$, s any integer.

If $\mathbf{R}$ has n independent eigenvalues, a similarity transformation can be found such that

$$\mathbf{Q}^{-1}\mathbf{R}\mathbf{Q} = \boldsymbol{\lambda} \tag{11}$$

where the columns of $\mathbf{Q}$ are the n-linearly independent eigenvectors of $\mathbf{R}$ and $\boldsymbol{\lambda}$ is a diagonal matrix whose elements are the eigenvalues of $\mathbf{R}$. Combining Eqs. (9) and (11) and using the definition of the matrix exponential[16] one has

$$\exp(\mathbf{R}T) = \mathbf{Q}\exp(\boldsymbol{\lambda}T)\mathbf{Q}^{-1}$$

or

$$\exp(\boldsymbol{\lambda}T) = \boldsymbol{\Lambda} = \mathbf{Q}^{-1}\Phi(T,0)\mathbf{Q} \tag{12}$$

where $\boldsymbol{\Lambda}$ is a diagonal matrix containing the eigenvalues of the transition matrix at the end of one period. The eigenvalues of $\Phi(T,0)$ or the characteristic multipliers are related to the eigenvalues of $\mathbf{R}$, denoted characteristic exponents, through the relation

$$\exp(\lambda_k T) = \Lambda_k \qquad k = 1, 2, \ldots n \tag{13}$$

Clearly λ_k and Λ_k are both complex quantities in general, thus

$$\begin{aligned} \zeta_k &= (1/2T)\ln[\Lambda_{kR}+\Lambda_{kI}{}^2] \\ \omega_k &= (1/T)\tan^{-1}(\Lambda_{kI}/\Lambda_{kR}) \end{aligned} \tag{14}$$

the quantity ω_k can be determined according to the Floquet-Liapunov theory only within an integer multiple of the nondimensional period.

The stability criteria for the system is related to the eigenvalues of $\mathbf{R}$ or the real part of the characteristic exponents ζ_k. The solutions of Eq. (6) approach zero as $\psi \to \infty$ if

$$|\Lambda_{kR}{}^2+\Lambda_{kI}{}^2| < 1 \quad \text{or} \quad \zeta_k < 0 \quad k = 1, 2, \ldots, n \tag{15}$$

From the preceding discussion it is clear that the efficient numerical computation of $\Phi(\mathbf{T}, 0)$ is the key to efficient treatment of periodic systems.

Calculation of the Transition Matrix $\Phi(T, 0)$

In the present study, the transition matrix at the end of a common period $\Phi(T, 0)$ is evaluated using two separate methods.

a) Direct Numerical Integration

This straightforward method[1,10] consists of evaluating the columns of $\Phi(T, 0)$, by integrating Eq. (6) n-times. Each integration yields one column $\Phi_k(\psi, \psi_o)$ of $\Phi(T, 0)$ corresponding to the initial conditions

$$y_j(\psi_o) = \begin{cases} 1 & j = k \\ 0 & j \neq k \end{cases} \tag{16}$$

The numerical integration was performed using a fourth-order Runge-Kutta method.

b) Approximate Method for Determining $\Phi(T, 0)$

In a recent series of papers, Hsu[3-5] has developed various methods for approximating the transition matrix during one period; the most efficient one consists of approximating the periodic matrix $\mathbf{A}(\psi)$ by a series of step functions, this method can be considered to be the generalization of the "rectangular ripple" method[6] to multidimensional systems. The method consists of evaluating the state transition matrix by dividing a period into a number of equal parts and considering the equations over each interval to be a set of constant coefficient equations. Because the method is new and numerically efficient, a description of its essential aspects is given below.

Each period T is divided into K intervals denoted by ψ_k, $k = 0, 1, 2 \ldots k$, with $0 = \psi_0 < \psi_1 < \ldots \psi_k = T$. In the kth interval the periodic coefficient matrix $A(\psi)$ is replaced by a constant matrix $\mathbf{C}(\psi)$ defined by

$$\mathbf{C}_k = \frac{1}{\Delta_k}\int_{\psi_{k-1}}^{\psi_k} \mathbf{A}(\xi)\,d\xi; \quad \Delta_k = \psi_k - \psi_{k-1}$$

with

$$\psi_k < \xi_k < \psi_{k-1} \tag{17}$$

Thus the actual system, Eq. (6), is approximated by an approximate system

$$\overset{*}{\mathbf{y}}_A(\psi; K) = \mathbf{C}(\psi; K)\mathbf{y}_A(\psi; K) \tag{18}$$

where $\mathbf{y}_A(0; K) = \mathbf{y}(0)$ and the subscript A denotes approximate quantities. The general expression for $\mathbf{C}(\psi, k)$ in terms of a series of step functions is given by

$$\mathbf{C}(\psi; K) = \sum_{s=-\infty}^{\infty}\sum_{k=1}^{K} \mathbf{C}_k[U(\psi-sT-\psi_{k-1}) - U(\psi-sT-\psi_k)] \tag{19}$$

The theory of differential equations with constant coefficients[16] enables one to write the fundamental matrix (or the transition matrix) of the system, with $\Phi_A(0; K) = \mathbf{I}$, as

$$\Phi_A(\psi; K) = \exp[(\psi-\psi_{k-1})\mathbf{C}_k]\exp(\mathbf{C}^{k-1}\Delta_{k-1})\ldots\exp(\mathbf{C}_1\Delta_1) \tag{20}$$

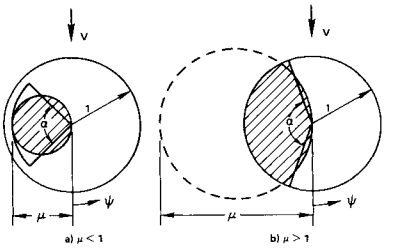

Fig. 2 Geometry of approximate and exact reversed flow regions.

from which $\Phi_A(T;K)$ is given by

$$\mathbf{H}(K) = \Phi_A(K) = \Phi_A(T;K) = \prod_{i=1}^{K} \exp(\Delta_i \mathbf{C}_i) \tag{21}$$

With regard to the product sign Π, it is understood that the order of positioning of the factors is material and the kth factor is to be placed in front of the $(k-1)$th factor. It can be shown[5] that when $K \to \infty$, $\mathbf{y}_A(\psi;K) \to \mathbf{y}(\psi)$ and $\Phi_A(\psi,K) \to \Phi(\psi,0)$ and $\Phi_A(K) = \Phi_A(T,0) \to \Phi(T,0)$.

The basic numerical problem is therefore the efficient computation of $\Phi_A(K)$. Using the definition of the matrix exponential[16]

$$\exp(\Delta_i \mathbf{C}_i) = \mathbf{I} + \Delta_i \mathbf{C}_i + \left(\frac{\Delta_i \mathbf{C}_i}{2!}\right)^2 + \cdots \left(\frac{\Delta_i \mathbf{C}_i}{n!}\right)^n$$
$$n = 1, 2, \ldots \infty \tag{22}$$

For small time intervals $\Delta_i \to 0$, the series in Eq. (22) converges rapidly, and the value of the matrix exponential can be accurately approximated by a finite number of terms. Thus

$$\exp(\Delta_i \mathbf{C}_i) \cong \mathbf{I} + \sum_{j=1}^{J} \left(\frac{\Delta_i \mathbf{C}_i}{j!}\right)^j = \exp(\Delta_i \mathbf{C}_i) - \sum_{j=J+1}^{\infty} \left(\frac{\Delta_i \mathbf{C}_i}{j!}\right)^j \tag{23}$$

Using the last equation the approximate value of the transition matrix at the end of the period can be rewritten as

$$\mathbf{H}_A(K) \cong \Phi_A(K) = \prod_{i=1}^{K} \left\{\mathbf{I} + \sum_{j=1}^{J} \left(\frac{\Delta_i \mathbf{C}_i}{j!}\right)^j\right\} \tag{24}$$

General error bounds for these approximations are obtained in Ref. 6. Furthermore, it can be shown the rate of convergence of the approximation is given by

$$\Phi(T,0) - \mathbf{H}_A(K) = \mathbf{0}(\Delta_i^{\,2}) \tag{25}$$

for $J \geq 2$.

Finally, it should be mentioned that for both methods used in evaluating $\Phi(T,0)$, the eigenvalues of the transition matrix were evaluated using a Jacobi-type eigenvalue routine.

Results and Discussion

Numerical Quantities Used in the Calculations

In computing the numerical results the following assumptions were made: 1) Mass and stiffness distribution was assumed to be constant along the span of the blade. 2) Two different kinds of mode shapes were used.

a) For the cases when essentially only a study of the properties of the numerical methods used (i.e., numerical experimentation) was conducted the mode shapes in flap and lag were approximated by the first nonrotating assumed mode shape used in Refs. 12 and 17. When this assumed mode shape was used, the elastic coupling effect, represented by the terms $\bar{E}_{11}{}^{s}$, $\bar{\bar{E}}_{11}{}^{s}$, $\bar{E}_{11}{}^{cs}$, $\bar{\bar{E}}_{11}{}^{cs}$ in the equations of motion, was neglected because the numerical accuracy of the method is independent of the data used in the calculations.

b) For all the cases, where a parametric investigation of typical hingeless rotor blade configurations was conducted, an exact rotating mode shape in flap and lag was employed. The exact rotating mode shapes were generated by using Galerkin's method based upon five nonrotating cantilever mode shapes for each flap or lag degree of freedom.[18] For these cases the elastic coupling effect was included. It should be noted that for the case of constant mass and stiffness distribution along the blade, there is a unique relationship between the first rotating and nonrotating frequencies in flap and lag, these relations are given in graphical form in Ref. 15.

The coefficients F^i, L^i, $\bar{B}^i \ldots P_{111}$, etc., were evaluated as described in Ref. 15. For the cases computed the inflow was evaluated using an expression for constant inflow ratio in *hover*, given by[17]

$$\lambda = (a\sigma/16)[(1+24\theta/a\sigma)^{1/2} - 1] \tag{26}$$

It should be emphasized that for forward flight a more complicated relation for the inflow should be used.[17] Use of such a relation introduces the requirement of changing the value of advance ratio μ, with the condition of trimmed flight at a fixed value of the thrust coefficient.[17] Experience gained using this approach[17] indicates that for this case it is difficult to determine which part of the degradation in stability is related to changes in collective and cyclic pitch, as dictated by the trim requirement, and which part is due to the periodic coefficients. In the present study which is aimed at determining the effect of the periodic coefficients this added complication was deemed to be unwarranted.

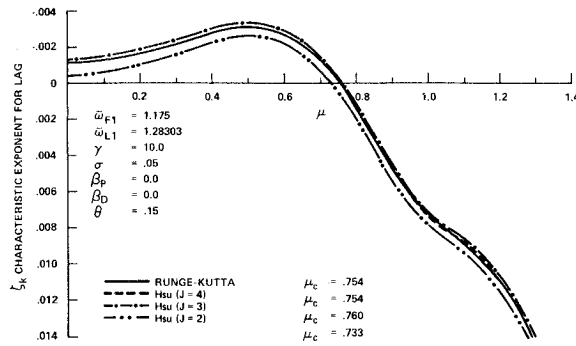

Fig. 3 Comparison of Runge-Kutta and Hsu's methods for a typical case.

Finally, in all the computations the following values were used:

$$C_{do} = 0.01; \quad a = 2\pi; \quad \sigma = 0.05; \quad e_1 = 0$$

Various other pertinent quantities are specified on the plots.

Results

Before proceeding with the description of the results it is important to note that Figs. 3–5 are based upon the assumed mode shape and for these cases the elastic coupling effect is neglected. The rest of the figures have been obtained using the exact rotating mode shapes and for these the elastic coupling effect is included.

Figure 3 shows the real part of the characteristic exponent as a function of the advance ratio. Starting the computation at $\mu = 0$, enables one to easily identify the instabilities encountered, by using results previously obtained for hover.[17] In Fig. 3, results for a typical case, obtained by evaluating $\Phi(T,0)$ by a fourth-order Runge-Kutta numerical integration, are compared with those obtained by evaluating $\mathbf{H}_A(T,0) \cong \Phi_A(T,0)$ from Eq. (24), with different orders of approximation (i.e., for different values of J). This plot shows that Runge-Kutta and Hsu's method using a fourth-order approximation to the solution of the constant coefficient equations in each interval give almost identical results. As shown, the lag degree of freedom becomes unstable for $\mu = 0.754$ and the frequency of oscillation is $\omega_k = 1.286$.

Figure 4 is a plot of the C.P.U. time required on an IBM

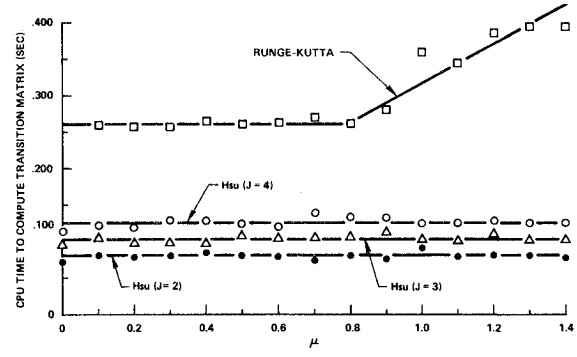

Fig. 4 Variation of CPU time to compute transition matrix with advance ratio.

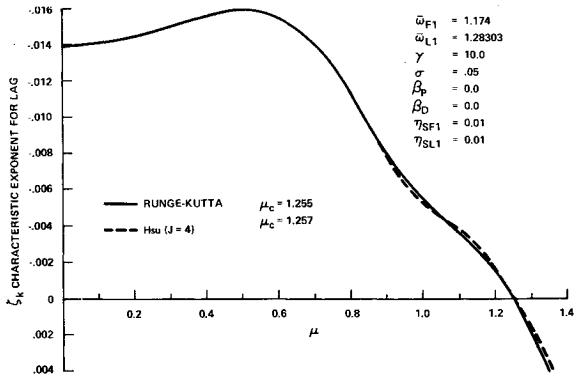

Fig. 5 Comparison of Runge-Kutta and Hsu's methods for a case with high μ_c.

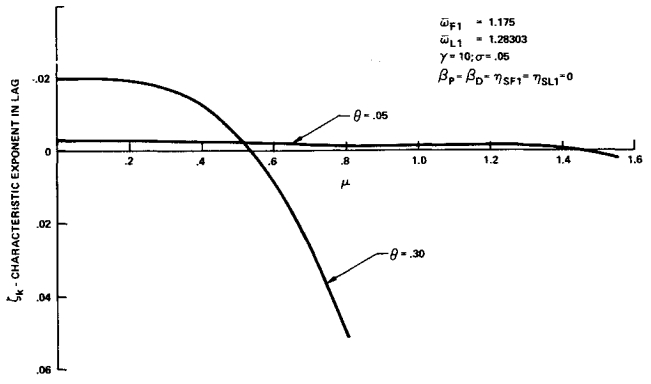

Fig. 7 Effect of collective pitch setting on a typical case.

360/91 computer to calculate the Floquet transition matrices for the four cases depicted in Fig. 3. As shown on the figure, Hsu's method, even using a fourth-order approximation, is computationally much more efficient than the fourth-order Runge-Kutta numerical integration scheme. The gradual increase in C.P.U. time for the Runge-Kutta method at $\mu = 0.8$ is associated with the piecewise continuity of the reversed flow region.

Figure 5 is a comparison of results between fourth-order Runge-Kutta and Hsu's method for a case that has a relatively high value of μ_c. Again the results compare favorably even for high values of μ.

Additional numerical experimentation indicated that the best results are obtained by dividing a blade revolution into a number of intervals between $35 < K < 50$.

The importance of the reversed flow region is illustrated by Fig. 6. As shown, with the reversed flow region the instability occurs at a higher value of μ than without the reversed flow region. Similar trends were observed in previous studies when only the flapping motion was considered,[9] indicating that by neglecting the reversed flow region one could expect conservative results from a stability point of view.

It is also clear from Fig. 6 that the difference in μ_c due to inclusion of the reversed flow region, for $\mu \cong 1.0$, is approximately 7%. Thus, the approximate representation of the reversed flow region, described in Appendix B, cannot significantly affect the accuracy of the results presented in this study.

It is also interesting to note from Fig. 6 that the reversed flow region becomes significant only for advance ratios greater than 0.7. Figure 6 also indicates that stability improves when the working part of the blade on the retreating side begins to become immersed in reversed flow.

The effect of collective pitch setting on blade stability is illustrated by Fig. 7 for the typical case $\omega_{F1} = 1.175$ and $\omega_{L1} = 1.28303$. As shown for a low value of collective pitch setting $\theta = 0.05$ the lag degree of freedom becomes unstable at $\mu_c = 1.435$ and $\omega_k = 1.279$. For a high value of collective pitch setting $\theta = 0.30$ the lag degree of freedom becomes unstable at $\mu_c = 0.535$ with a frequency of $\omega_k = 1.332$. These results seem to indicate that the use of a trim procedure, such as developed in Ref. 17, will be required in realistic stability calculations in forward flight. Furthermore, it seems that the assumption of nonlifting rotors used in some forward flight studies can be nonconservative.

Figure 8 illustrates the effect of the Lock number, based on normal flow, on the stability of the blade in forward flight. As shown, an increase in the value of γ tends to destabilize the blade in the lag degree of freedom. For $\gamma = 5.0$ the lag degree of freedom becomes unstable at $\mu_c = 1.425$ and $\omega_k = 1.283$, for $\gamma = 10.0$ the lag degree of freedom becomes unstable at $\mu_c = 0.583$ and $\omega_k = 1.295$, and for $\gamma = 15.0$ the lag degree of freedom becomes unstable at $\mu_c = 0.568$ and $\omega_k = 1.294$.

Hingeless helicopter blades are usually designed with a first rotating flap frequency of $1.1 \leqq \bar{\omega}_{F1} \leqq 1.2$. Thus the value of $\bar{\omega}_{F1} = 1.175$ used in the numerical calculations can be considered to be a representative value for this parameter. On the other hand the rotating lag frequency for hingeless blades has usually a considerable variation, therefore it is reasonable to investigate the effect of changing this parameter over a wide range such as $0.2 \leqq \bar{\omega}_{L1} \leqq 2.5$; the results are presented in Fig. 9.

First it should be noted that two kinds of instabilities are shown in Fig. 9: those associated with flap degree of freedom marked by squares, and those associated with the lag degree of freedom marked by circles. As shown at least for half of the cases, the triggering mechanism for the instability is associated with the lag degree of freedom. Thus the lag degree of freedom should be included in blade stability and response calculations in forward flight and probably the same is true for the torsional degree of freedom.

Furthermore, Fig. 9 also illustrated that the instabilities which occur are usually characterized by two distinct types of frequencies:

a) those for which the imaginary part of the characteristic exponent is equal to 0, $\frac{1}{2}$, or 1 indicating that the instability is

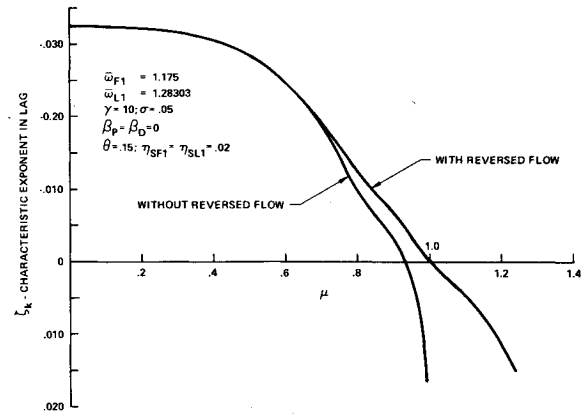

Fig. 6 Effect of reversed flow on the characteristic exponent for lag.

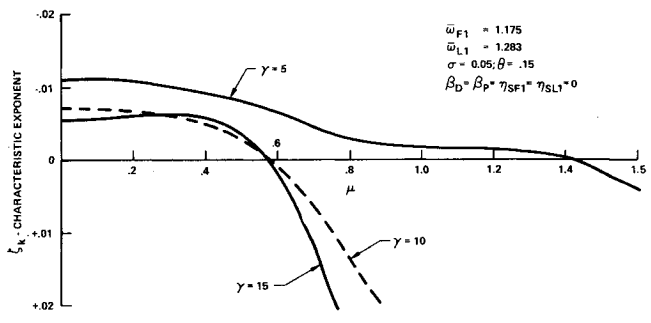

Fig. 8 Effect of lock number on characteristic exponent for lag.

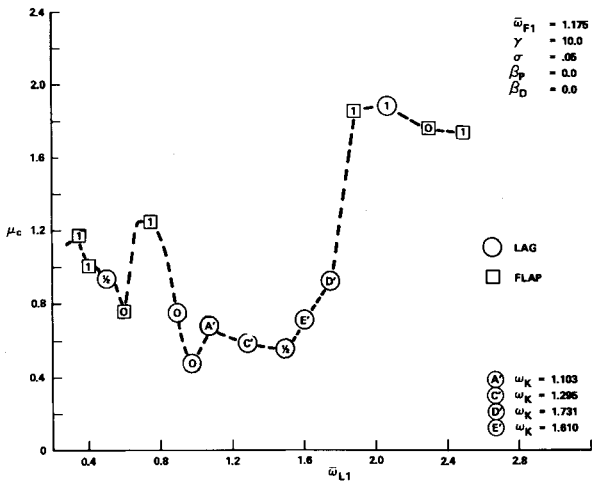

Fig. 9 Effect of variation in rotating lag frequency on μ_c.

directly due to the periodic coefficients in the system, for these points the appropriate number appears inside the circles or squares indicating the stability boundary; and

b) those for which ω_k has a continuous value, usually close to the rotating lag frequency, marked by letters A', B', C' etc. For these points the instability is due to an aerodynamic coupling term associated with the lag equation described in Ref. 15.

As can be seen from Fig. 9 there are two regions where degradation of stability can be expected with forward flight. One region is between $0.9 \leqq \bar{\omega}_{L1} \leqq 1.6$. While a second and much smaller region is between $0.45 < \bar{\omega}_{L1} < 0.55$, the detrimental effect of forward flight for this region has been predicted also from purely mathematical considerations.[12]

The results presented in Fig. 9 seem to indicate that at high advance ratios a soft inplane hingeless blade with $0.7 < \bar{\omega}_{L1} < 0.8$ will be the most stable; while for a stiff inplane hingeless blade a lag frequency of $\bar{\omega}_{L1} > 1.6$ would be the best.

Finally, it should be noted that, although the points in Fig. 9 have been connected by lines, a possibility exists that additional flutter points which could be evaluated between the calculated points may not be exactly on the lines as drawn, this is due to the periodicity of the coefficients in the equations of motion.

Conclusions

The major conclusions obtained from the present study are summarized below. They should be considered indicative of trends and their application to the design of a helicopter blade should be limited by the assumptions used.

1) Hsu's method for calculating the Floquet transition matrix at the end of a period is a powerful computational scheme which represents a significant improvement over previous methods. Compared to direct numerical integration, Hsu's method was approximately 2.5 times faster for a system of four first-order equations. For larger systems, it probably could be more efficient by a factor of n, where n is the size of the $\mathbf{A}(\psi)$ matrix. Multivariable Floquet-Liapunov theory coupled with Hsu's method is a general and efficient tool for determining the stability of periodic aeroelastic systems.

2) Flapping instability and response studies at high advance ratios can be inaccurate and misleading because of the neglect of the lead-lag degree of freedom. The effect of the periodic coefficients on the coupled flap-lag system shows that, in general, instability can occur at lower values of advance ratios than when the flap degree of freedom is considered by itself.

3) The value of the collective pitch setting has a considerable effect on the value of the advance ratio at which instabilities due to the periodic coefficients or the aerodynamic coupling terms occur. An increase in collective pitch is destabilizing, therefore high advance ratio studies which do not include this effect (nonlifting rotors) may yield nonconservative results.

4) The results obtained seem to indicate that certain values of rotating lag frequencies can provide improved aeroelastic performance for hingeless blades at high advance ratios.

Appendix A: Elements of the A-Matrix and Definition of Various Quantities

The elements of the $\mathbf{A}(\psi)$-matrix, which defines the equations of motion when written as first-order differential equations, are given below

$$A_{21} = 1; \quad A_{22} = A_{23} = A_{24} = 0$$

$$A_{23} = 1; \quad A_{41} = A_{42} = A_{44} = 0$$

$$A_{11} = -2\eta_{SF1}\bar{\omega}_{F1} + \frac{1}{\bar{M}_{F1}}\left\{\frac{\gamma}{2}\left(\frac{l}{R}\right)^2\left[-F^8\frac{l}{R} - F^9\mu\frac{l}{R}\sin\psi + F^{24}\mu\cos\psi\frac{l}{R}h_1{}^o\right]\right\}$$

$$A_{12} = -\bar{\omega}_{F1}{}^2 + \frac{1}{\bar{M}_{F1}}\left\{-\bar{E}^s + \frac{\gamma}{2}\left(\frac{l}{R}\right)^2\left[-F^6\mu\cos\psi - F^7\frac{\mu^2}{2}\sin 2 + F^{23}\frac{\mu^2}{2}(1+\cos 2\psi)h_1{}^o\right]\right\}$$

$$A_{13} = \frac{1}{\bar{M}_{F1}}\left\{2\bar{P}_{111}g_1{}^o + 2(\beta_P+\beta_D)\bar{B}_{11}{}^3 + \frac{\gamma}{2}\left(\frac{l}{R}\right)^2\left[-F^{10}2\frac{l}{R}\theta - F^{11}\frac{l}{R}2\theta\sin\psi + F^{11}\frac{l}{R}\cos\psi\mu(\beta_P+\beta_D) + F^{11}\lambda\frac{l}{R} + F^{14}\frac{l}{R}\mu\cos\psi g_1{}^o\right]\right\}$$

$$A_{14} = \frac{\bar{E}^{cs}}{\bar{M}_{F1}} + \frac{\gamma}{2}\left(\frac{l}{R}\right)^2\left\{\theta(-2F^{21}\mu\cos\psi - \mu^2\sin 2\psi F^{22}) + \lambda\mu F^{22}\cos\psi + \frac{\mu^2}{2}(1+\cos 2\psi)[F^{23}g_1{}^o + F^{22}(\beta_P+\beta_D)]\right\}\frac{1}{\bar{M}_{F1}}$$

$$A_{31} = \frac{1}{\bar{M}_{L1}}\left\{-(2\bar{M}_\eta)_{111}g_1{}^o - 2(\beta_P+\beta_D)\bar{B}_{11}{}^7 + \frac{\gamma}{2}\left(\frac{l}{R}\right)^2\left[L^7\frac{l}{R}\theta + L^8\frac{l}{R}\mu\theta\sin\psi - L^8 2\mu\frac{l}{R}\cos\psi(\beta_P+\beta_D) - L^8 2\lambda\frac{l}{R} - L^{17}2\frac{l}{R}\mu\cos\psi g_1{}^o - L^{22}\frac{l}{R}\mu\cos\psi\theta h_1{}^o\right]\right\}$$

$$A_{32} = \frac{\bar{\bar{E}}_{cs}}{\bar{M}_{L1}} + \frac{\gamma}{2}\left(\frac{l}{R}\right)^2\left[\theta\left(\frac{\mu^2}{2}L^{11}\sin 2\psi + L^{10}\mu\cos\psi\right) - 2\lambda L^{11}\mu\cos\psi - \frac{\mu^2}{2}\theta(1+\cos 2\psi)L^{21}h_1{}^o - \mu^2(\beta_P+\beta_D)L^{11}(1+\cos 2\psi) - L^{24}\mu^2 g_1{}^o(1+\cos 2\psi)\right]\frac{1}{\bar{M}_{L1}}$$

$$A_{33} = -2\eta_{SL1}\bar{\omega}_{L1} + \frac{1}{\bar{M}_{L1}}\left\{h_1{}^o[2\bar{S}_{111} - 2(\bar{M}_y)_{111}] + \frac{\gamma}{2}\left(\frac{l}{R}\right)^2\left[-L^{13}\mu\cos\psi(\beta_P+\beta_D)\frac{l}{R}\theta - L^{13}2\mu\sin\psi\frac{l}{R}\frac{C_{do}}{a} - L^{14}2\frac{l}{R}\frac{C_{Do}}{a} - L^{13}\lambda\frac{l}{R}\theta - L^{16}\mu\cos\psi\frac{l}{R}\theta g_1{}^o\right]\right\}$$

$$A_{34} = -\left(\bar{\omega}_{L1}{}^2 - \frac{\bar{\bar{E}}^s}{\bar{M}_{L1}}\right) + \frac{\gamma}{2}\left(\frac{l}{R}\right)^2 \left\{ -\theta\lambda\mu L^{20}\cos\psi + \frac{\mu^2}{2}(1+\cos 2\psi)[-L^{21}g_1{}^o - (\beta_P+\beta_D)L^{20}]\theta + \frac{C_{Do}}{a}(-\mu^2 L^{20}\sin 2\psi - 2\mu L^{23}\cos\psi)\right\} \Big/ \bar{M}_{L1}$$

For completeness, the definition of the various quantities used in the equations presented above is briefly described.

The quantities $\bar{M}_{F1}$, $\bar{M}_{L1}$, $\bar{P}_{111}$, $\bar{S}_{111}$, $(\bar{M}_\gamma)_{111}$, $\bar{B}^i$ are generalized mass integrals defined in Refs. 12, 15, and 17.

The quantities F^i, L^i are aerodynamic integrals associated with the generalized aerodynamic forces A_{F1} and A_{L1} defined in Ref. 15.

The quantities $\bar{E}_{11}{}^s$, $\bar{E}_{11}{}^{cs}$, $\bar{\bar{E}}_{11}{}^s$, and $\bar{\bar{E}}_{11}{}^{cs}$ are elastic coupling terms due to the collective pitch setting of the blade defined in Ref. 15. Finally, the quantities $g_1{}^o$ and $h_1{}^o$ are the steady-state deflections at the tip of the blade in hover, defined in Ref. 15.

Appendix B: Approximate Representation of the Reversed Flow Region

The approximate reversed flow model developed for the present study consists of replacing the circular region[7] by an approximate region which is a circular sector as shown in Fig. 2. The approximation is based on the assumption that the area contained in the circular sector must be equal to the area contained in the approximate region. Two separate cases must be considered: 1) $\mu < 1$, 2) $\mu \geqq 1$.

Case 1: For $\mu < 1$, the radius of the circular part is taken as μ. Simple geometric considerations show that the angle α is always a constant, given by $\alpha = \pi/2$.

Case 2: For $\mu \geqq 1$ simple geometric considerations show that

$$\alpha = \pi - 2\sin^{-1}(1/\mu) + \mu^2 \sin^{-1}(1/\mu) - (\mu^2-1)^{1/2}$$

The generalized aerodynamic forces A_{F1}, A_{L1} in the reversed flow region are evaluated using the assumption that the lift curve slope in the reversed flow region is equal to the negative value of the lift curve slope in normal flow.[15]

References

[1] Hohenemser, K. H. and Yin, S. K., "Some Applications of the Method of Multiblade Coordinates," *Journal of the American Helicopter Society*, Vol. 17, No. 3, 1972, pp. 3–12.

[2] Dzygadlo, Z., "Parametric Self-Excited Vibration of a Simple Supported Plate in Supersonic Flow," *Proceedings of Vibration Problems* (Warsaw), Vol. 4, No. 6, 1965, pp. 381–394.

[3] Hsu, C. S., "Impulsive Parametric Excitation: Theory," *Journal of Applied Mechanics*, Vol. 39, No. 2, 1972, pp. 551–558.

[4] Hsu, C. S. and Cheng, W. H., "Applications of the Theory of Impulsive Parametric Excitation and New Treatments of General Parametric Excitation Problems," *Journal of Applied Mechanics*, Vol. 40, No. 1, 1973, pp. 78–86.

[5] Hsu, C. S., "On Approximating a General Linear Periodic System," *Journal of Mathematical Analysis and Applications*, to be published; also presented as a paper in the International Congress of Applied Mechanics, Moscow, 1972.

[6] Horvay, G. and Yuan, S. W., "Stability of Rotor Blade Flapping Motion when the Hinges are Tilted. Generalization of the 'Rectangular Ripple' Method of Solution," *Journal of the Aeronautical Sciences*, Vol. 14, No. 10, 1947, pp. 583–593.

[7] Sissingh, G. J., "Dynamics of Rotors Operating at High Advance Ratios," *Journal of the American Helicopter Society*, Vol. 13, No. 3, 1968, pp. 56–63.

[8] Sissingh, G. J. and Kuczynski, W. A., "Investigations on the Effect of Blade Torsion on the Dynamics of the Flapping Motion," *Journal of the American Helicopter Society*, Vol. 15, No. 2, 1970, pp. 2–9.

[9] Lowis, O. J., "The Stability of Rotor Blade Flapping Motion at High Tip Speed Ratios," Reports and Memoranda 3544, Jan. 1963, Aeronautical Research Council, London, England.

[10] Peters, D. A. and Hohenemser, K. H., "Application of the Floquet Transition Matrix to Problems of Lifting Rotor Stability," *Journal of the American Helicopter Society*, Vol. 16, No. 2, 1971, pp. 25–33.

[11] Johnson, W., "A Perturbation Solution of Rotor Flapping Stability," AIAA Paper 72-955, Palo Alto, Calif., 1972.

[12] Friedmann, P. and Tong, P., "Nonlinear Flap-Lag Dynamics of Hingeless Helicopter Blades in Hover and in Forward Flight," *Journal of Sound and Vibration*, Vol. 30, No. 1, 1973, pp. 9–31.

[13] Hall, W. E., "Application of Floquet Theory to the Analysis of Rotary Wing VTOL Stability," SUDDAR 400, Feb. 1970, Stanford University Center for Systems Research, Palo Alto, Calif.

[14] Crimi, P., "A Method for Analyzing the Aeroelastic Stability of a Helicopter Rotor in Forward Flight," CR-1332, Aug. 1969, NASA.

[15] Friedmann, P. and Silverthorn, L. J., "Aeroelastic Stability of Coupled Flap-Lag Motion of Hingeless Helicopter Blades at Arbitrary Advance Ratios," CR-132 431, Feb. 1974, NASA; also UCLA-ENG-7406, Feb. 1974, Univ. of California at Los Angeles, Los Angeles, Calif.

[16] Brockett, R. W., *Finite Dimensional Linear Systems*, Wiley, New York, 1970, pp. 19–38.

[17] Friedmann, P. and Tong, P., "Dynamic Nonlinear Elastic Stability of Helicopter Rotor Blades in Hover and Forward Flight," ASRL TR 166-3, (NASA CR-114485), June 1972, MIT, Cambridge, Mass.

[18] Yntema, R. T., "Simplified Procedures and Charts for the Rapid Estimation of Bending Frequencies of Rotating Beams," TN 3459, 1955, NACA.